The prospects for constraining dark energy with future X-ray cluster gas mass fraction measurements

David Rapetti[1*] and Steven W. Allen[1]
[1] *Kavli Institute for Particle Astrophysics and Cosmology at*
Stanford University, 382 Via Pueblo Mall, Stanford 94305-4060, CA, USA, and
Stanford Linear Accelerator Center, 2575 Sand Hill Road, Menlo Park 94025, CA, USA.

ABSTRACT

We examine the ability of a future X-ray observatory, with capabilities similar to those planned for the Constellation-X mission, to constrain dark energy via measurements of the cluster X-ray gas mass fraction, f_{gas}. We find that f_{gas} measurements for a sample of ~ 500 hot ($kT \gtrsim 5\,\mathrm{keV}$), X-ray bright, dynamically relaxed clusters, to a precision of ~ 5 per cent, can be used to constrain dark energy with a Dark Energy Task Force (DETF; Albrecht et al. 2006) figure of merit of $20 - 50$. Such constraints are comparable to those predicted by the DETF for other leading, planned 'Stage IV' dark energy experiments. A future f_{gas} experiment will be preceded by a large X-ray or SZ survey that will find hot, X-ray luminous clusters out to high redshifts. Short 'snapshot' observations with the new X-ray observatory should then be able to identify a sample of ~ 500 suitably relaxed systems. The redshift, temperature and X-ray luminosity range of interest has already been partially probed by existing X-ray cluster surveys which allow reasonable estimates of the fraction of clusters that will be suitably relaxed for f_{gas} work to be made; these surveys also show that X-ray flux contamination from point sources is likely to be small for the majority of the targets of interest. Our analysis uses a Markov Chain Monte Carlo method which fully captures the relevant degeneracies between parameters and facilities the incorporation of priors and systematic uncertainties in the analysis. We explore the effects of such uncertainties, for scenarios ranging from optimistic to pessimistic. We conclude that the f_{gas} experiment offers a competitive and complementary approach to the best other large, planned dark energy experiments. In particular, the f_{gas} experiment will provide tight constraints on the mean matter and dark energy densities, with a peak sensitivity for dark energy work at redshifts midway between those of supernovae and baryon acoustic oscillation/weak lensing/cluster number counts experiments. In combination, these experiments should enable a precise measurement of the evolution of dark energy.

Key words: cosmology:observations – cosmology:cosmological parameters – cosmology:theory – x-ray clusters – dark energy

1 INTRODUCTION

In the early 1990s, measurements of the baryonic mass fraction in X-ray luminous galaxy clusters provided compelling evidence that we live in a low density Universe. Under the assumption that large clusters provide approximately fair samples of the matter content of the Universe, X-ray observations require that the mean matter density, Ω_m, is significantly less than the critical value, with a best-fit value $\Omega_m \sim 0.2 - 0.3$ (e.g. White & Frenk 1991; Fabian 1991; Briel

et al. 1992; White et al. 1993; David et al. 1995; White & Fabian 1995; Evrard 1997; Mohr et al. 1999; Ettori & Fabian 1999; Roussel et al. 2000; Grego et al. 2001; Allen et al. 2002, 2004, 2007; Ettori et al. 2003; Sanderson & Ponman 2003; Lin et al. 2003; LaRoque et al. 2006). When combined with the expectation from inflation models, later confirmed by Cosmic Microwave Background (CMB) studies (Bennett et al. 2003; Spergel et al. 2003, and references therein), that the Universe should be close to spatially flat, X-ray results on the cluster baryon mass fraction quickly lead to the suggestion that the mass-energy density of the Universe may

* Email: drapetti@slac.stanford.edu

be dominated by a cosmological constant (e.g. White et al. 1993).

The first direct evidence for late-time cosmic acceleration, as would be produced by a sizeable cosmological constant, was provided in the late 1990s by Riess et al. (1998) and Perlmutter et al. (1999) based on measurements of the light curves of type Ia supernovae (SNIa). Since then, larger SNIa data sets (Knop et al. 2003; Riess et al. 2004; Astier et al. 2005; Riess et al. 2007; Wood-Vasey et al. 2007; Davis et al. 2007) and an increasingly wide array of other, complementary experiments, have confirmed and improved upon this striking measurement. The combination of CMB data from the Wilkinson Microwave Anisotropy Probe (WMAP) (Spergel et al. 2003; Spergel et al. 2006) with large scale structure (LSS) data from the Sloan Digital Sky Survey (SDSS) (Eisenstein et al. 2005; Percival et al. 2007) and/or 2dF Galaxy Redshift Survey (2dFGRS) (Cole et al. 2005) provides powerful evidence for dark energy. The cross-correlation of CMB and LSS fluctuations reveals the effects of dark energy on the Integrated Sachs-Wolfe effect (Scranton et al. 2003; Fosalba et al. 2003; Rassat et al. 2007). Measurements of the amplitude and evolution of matter fluctuations using X-ray galaxy clusters (Reiprich & Böhringer 2002; Allen et al. 2003; Schuecker et al. 2003; Voevodkin & Vikhlinin 2004; Mantz et al. 2007; Borgani et al. 2001; Henry 2004), optically-selected clusters (Gladders et al. 2007; Rozo et al. 2007), Lyman-α forest data (Viel et al. 2004; Seljak et al. 2005), and weak lensing (Van Waerbeke et al. 2005; Jarvis et al. 2005; Hoekstra et al. 2006; Benjamin et al. 2007), also provide important, powerful confirmation of the new, standard cosmological paradigm: a universe in which the main mass and energy components are dark matter and dark energy, and where dark energy drives the current acceleration. The standard model for dark energy remains the cosmological constant, which is mathematically equivalent to vacuum energy. In principle, however, cosmic acceleration could be driven by either dark energy or a modification to the laws of gravity on cosmological scales (see Copeland et al. 2006, for an extensive review).

Building on the early X-ray work, Allen et al. (2004); Rapetti et al. (2005); Allen et al. (2007) showed that measurements of the evolution of the X-ray gas mass fraction, f_{gas}, in the largest, dynamically relaxed galaxy clusters provides a further powerful, complementary approach for studying dark energy. As with SNIa data, $f_{gas}(z)$ measurements probe the redshift-distance relation: whereas the peak SNIa luminosity varies as the square of the distance, f_{gas} measurements vary as distance, $d^{1.5}$ (the distance dependance derives from the way in which f_{gas} values are determined from the observed X-ray temperature and surface brightness data; Allen et al. 2007). In combination with the tight constraint on Ω_m provided by the normalization of the $f_{gas}(z)$ curve, under the assumption of fair matter samples, the $f_{gas}(z)$ data contain sufficient information to break the degeneracy between Ω_m and the dark energy equation of state, w, in the distance equations. The additional combination of f_{gas} and CMB data breaks other important degeneracies between parameters in cosmological analyses (Rapetti et al. 2005; Allen et al. 2007).

Allen et al. (2007) show that the current constraints on dark energy from the f_{gas} experiment are of comparable precision to other leading techniques, and are robust under the inclusion of conservative systematic allowances e.g. relaxing the requirement for exact hydrostatic equilibrium and allowing for moderate redshift evolution in the cluster baryon fraction. These authors also show that intrinsic, systematic scatter remains undetected in the current f_{gas} data, despite a weighted mean statistical scatter in the individual distance measurements of only ~ 5 per cent; in contrast, SNIa studies (Riess et al. 2007; Jha et al. 2007; Wood-Vasey et al. 2007) have established the presence of systematic scatter at the ~ 7 per cent in distance measurements from the best current SNIa data.

The key to determining the nature of dark energy is to obtain precise measurements of its evolution with redshift, z, or scale factor, $a = 1/(1+z)$. The Dark Energy Task Force report (Albrecht et al. 2006, hereafter DETF) presented estimates of the constraints on dark energy parameters that should be achievable with a number of future proposed or planned dark energy experiments. In particular, the report forecasted the ability of these experiments, in combination with CMB data from the Planck satellite, to constrain a dark energy model of the form $w(a) = w_0 + w_a(1 - a)$, and defined a figure of merit (hereafter FoM) to allow for easy comparison of the constraints. In this paper, we use the same dark energy parameterization and FoM to quantify the constraining power of future f_{gas} experiments, to be carried out with e.g. the Constellation-X or X-ray Evolving Universe Spectroscopy (XEUS) missions, in combination with CMB data. We show that the f_{gas} experiment is likely to provide comparable constraining power to the best other, contemporary space and ground-based experiments described by the DETF. When combined, future CMB, SNIa, baryon acoustic oscillation (BAO), weak lensing, cluster number count and f_{gas} experiments should provide precise, accurate constraints on $w(z)$ and allow significant progress in understanding the origin of cosmic acceleration.

The structure of this paper is as follows: in Section 2 we define the dark energy model and the FoM. In Section 3 we describe the simulated f_{gas} and CMB data sets. For the f_{gas} data, we assume instrument characteristics appropriate for the baseline Constellation-X mission. The CMB data set approximates that expected from two years of Planck data. We also simulate a data set representative of that produced by follow-up observations of the Sunyaev-Zel'dovich effect in the clusters targeted for the f_{gas} work. Section 4 describes the Markov Chain Monte Carlo (MCMC) pipeline and details of the analysis method. Our main results are presented in Section 5. Section 6 summarizes our conclusions.

2 THE DARK ENERGY MODEL AND FOM

We characterize the evolution of dark energy by its energy density in units of the critical density, Ω_{de}, and its equation of state, w. Following the DETF, we parameterize the evolution of the dark energy equation of state as $w(a) = w_0 + w_a(1 - a)$ (Chevallier & Polarski 2001; Linder 2003) for which a cosmological constant has $w(a) = -1$. In this model, the dimensionless Hubble parameter as a function of scale factor has the form

$$E(a) = \frac{H(a)}{H_0} = \sqrt{\Omega_m a^{-3} + \Omega_{de} f(a) + \Omega_k a^{-2}}, \qquad (1)$$

where

$$f(a) = a^{-3(1+w_0+w_\mathrm{a})} e^{-3w_\mathrm{a}(1-a)} \,. \qquad (2)$$

H_0 is the present-day value of the Hubble parameter and Ω_m and Ω_k are the mean matter density and curvature density in units of the critical density, respectively.

Using this parameterization, the DETF define a FoM that is used to compare the constraining power of different dark energy experiments. Nominally, the FoM scales with the inverse of the area enclosed by the 95 per cent confidence contour in the $w_0 - w_\mathrm{a}$ plane. However, the DETF showed that since there is little correlation in the $w_\mathrm{p} - w_\mathrm{a}$ plane, the area is also proportional to the product of the standard deviations $\sigma(w_\mathrm{p}) \times \sigma(w_\mathrm{a})$, where $w_\mathrm{p} = w(a_\mathrm{p})$ is the pivot value of $w(a)$ i.e. the value of $w(a)$ at which its uncertainty is minimized (Linder 2006). (Note that the standard error $\sigma(w_\mathrm{p})$ approximately corresponds to the 68.3 per cent uncertainty in w that would be obtained for a constant$-w$ dark energy model). This leads to the definition

$$\mathrm{FoM} = [\sigma(w_\mathrm{p}) \times \sigma(w_\mathrm{a})]^{-1} \,. \qquad (3)$$

For the DETF Fisher matrix analysis, the 1σ confidence region in the $w_\mathrm{p} - w_\mathrm{a}$ plane forms an ellipse for which the semi-axes are the standard deviations of w_p and w_a. For the more detailed MCMC analysis used here, however, we obtain slightly asymmetric probability distributions for these parameters in some cases, although to either side of the peak probability the distributions can be modelled as approximately Gaussian. Therefore, in calculating the FoM, we model the 1σ confidence contour in the $w_\mathrm{p} - w_\mathrm{a}$ plane with a geometrical shape formed by four quarters of four different ellipses for which the semi-axes are the standard deviations of the Gaussians to either side of the peak, namely $\sigma_\mathrm{up}(w_\mathrm{p})$, $\sigma_\mathrm{down}(w_\mathrm{p})$, $\sigma_\mathrm{up}(w_\mathrm{a})$, and $\sigma_\mathrm{down}(w_\mathrm{a})$. The area of such contour is equivalent to the area of an ellipse with semi-axes $\hat{\sigma}(w_\mathrm{p}) = [\sigma_\mathrm{up}(w_\mathrm{p}) + \sigma_\mathrm{down}(w_\mathrm{p})]/2$ and $\hat{\sigma}(w_\mathrm{a}) = [\sigma_\mathrm{up}(w_\mathrm{a}) + \sigma_\mathrm{down}(w_\mathrm{a})]/2$. Thus, we calculate our FoM [1] as the inverse of the product of the semi-axes $[\hat{\sigma}(w_\mathrm{p}) \times \hat{\sigma}(w_\mathrm{a})]^{-1}$ which allows a direct comparison with the results reported by the DETF.

3 SIMULATED X-RAY DATA

3.1 A strategy for future f_gas work

We assume that a future f_gas experiment will be carried out by an X-ray observatory with capabilities comparable to those of Constellation-X, as summarized in Table 1. The major improvements of such a mission with respect to current X-ray observatories are in collecting area, which is a factor ~ 100 larger than that provided by the Chandra X-ray Observatory, and spectral resolution. [2] We assume that

Table 1. Baseline X-ray observatory characteristics.

Band pass	0.3-10 keV
Spectral resolution	$E/\Delta E \sim 2400$ (@6 keV)
Effective area	$15{,}000$ cm^2 (@1.25 keV)
PSF	$\leqslant 15$ arcsec (half power diameter)
Field of View	$\geqslant 5 \times 5$ arcmin^2

the f_gas experiment will be preceded by, and will build upon, forthcoming X-ray and/or SZ cluster surveys[3] that will scan a significant fraction of the sky and find large number of hot, X-ray luminous, high$-z$ clusters. These surveys will provide the initial target lists for the f_gas experiment as well as allowing an array of complementary cosmological tests based on the power spectrum and mass function of galaxy clusters (e.g. Albrecht et al. 2006).

From initial surveys of tens of thousands of clusters, the ~ 3000 most X-ray luminous (or highest integrated SZ flux) clusters will be identified. The new X-ray observatory will then be used to take short snapshot exposures (~ 1ks) of these clusters, to identify the most apparently dynamically relaxed systems that are most suitable for f_gas work (Allen et al. 2007). The selection of relaxed clusters is likely to be based primarily on X-ray morphology, but will also utilize the high spectral resolution capabilities to measure bulk gas motions.[4] The most relaxed clusters will be re-observed with deeper exposures to measure the gas mass fraction to the required level of precision.

Current studies of the Massive Cluster Survey (MACS) (Ebeling et al. 2001, 2007) show that at redshifts $z \lesssim 0.5$ approximately 1/4 clusters are sufficiently relaxed for f_gas work (Allen et al. 2007). We (conservatively) calculate predicted cosmological constraints for two separate f_gas data sets, containing either ~ 500 or 250 relaxed clusters. That is, we assume that only approximately 1/6 or 1/12 of the 3000 hottest, most X-ray luminous clusters detected in a future survey will be suitable for use in the f_gas experiment.

For the $500-$cluster sample, we assume an average exposure time per cluster of ~ 20ks. For the $250-$cluster sample, the typical exposure is ~ 40ks. In both cases, the total time required to complete the f_gas observations will be $\lesssim 15$Ms. For the assumed instrument characteristics, we expect statistical uncertainties in the f_gas measurements resulting from 20ks exposures of ~ 5 per cent, which corresponds to ~ 3.3 per cent in distance. For typical exposures of 40ks, we expect to measure f_gas to ~ 3.5 per cent or distance to ~ 2.3 per cent. In Section 5 we show that the constraints on dark energy from both the 500 or 250-cluster

---

[1] To confirm the validity of our definition of the FoM we have explicitly measured the area contained by the filled contours in the right panel of Figure 2. Dividing this area by both the geometric factor π, which accounts for the conversion between the area of an ellipse and its circumscript rectangle, and the factor 2.3, which accounts for the change in the confidence levels from two to one degrees of freedom, we successfully match the measured area to the value obtained by the product $\hat{\sigma}(w_\mathrm{p}) \times \hat{\sigma}(w_\mathrm{a})$.

[2] For details on planned X-ray observatories see http://constellation.gsfc.nasa.gov/ and http://www.rssd.esa.int/index.php?project=XEUS.

[3] Forthcoming X-ray survey missions include Spectrum-RG/eROSITA; see http://www.mpe-garching.mpg.de/projects.html#erosita and http://www.mpe-garching.mpg.de/erosita/MDD-6.pdf. Several large-area SZ surveys are already underway, including the South Pole Telescope (SPT) (e.g. Ruhl et al. 2004, see http://spt.uchicago.edu/), and the Atacama Cosmology Telescope (ACT) (e.g. Sehgal et al. 2007, see http://wwwphy.princeton.edu/act/).

[4] The snapshot observations will also be of great benefit for a range of ancillary cluster science.

sample are comparable. We adopt the $500-$cluster sample with 5 per cent f_{gas} measurement uncertainties as our default data set.

3.2   The simulated f_{gas} data set

3.2.1   *The luminosity function of clusters*

To simulate the f_{gas} data set, we first need to predict the redshift distribution of clusters. We assume an X-ray flux-limited cluster survey similar to that expected to be produced by the Spectrum-RG/eROSITA mission, with a flux limit of $F_{\mathrm{lim}} = 3.3 \times 10^{-14}\,\mathrm{erg\,cm^{-2}\,s^{-1}}$ in the $0.1 - 2.4\,\mathrm{keV}$ band and a uniform sky coverage of $f_{\mathrm{sky}} \sim 0.5$. We calculate the number of clusters expected to be observed N_{i} in each redshift bin z_{i} as (Mantz et al. 2007)

$$N_{\mathrm{i}}(z_{\mathrm{i}}) = \int_{z_{\mathrm{i}-1}}^{z_{\mathrm{i}}} \frac{dV}{dz}\, dz \int_{0}^{\infty} \frac{dn(M,z)}{dM} Q\, dM \,, \tag{4}$$

where

$$Q = \int_{0}^{\infty} dL' \int_{L_{\mathrm{lim}}(z)}^{\infty} dL\, P(L'|M)\, p(L|L'). \tag{5}$$

Here, V is the comoving volume, $n(M, z)$ is the number density of halos with a mass less than M at redshift z, L' is the intrinsic luminosity of a galaxy cluster associated with a halo of mass M, and L is its detected luminosity. $P(L'|M)$ is the probability for a cluster of mass M to have an intrinsic luminosity L'; $p(L|L')$ is the probability for a cluster with intrinsic luminosity L' to be detected with luminosity L; and L_{lim} is the luminosity limit function. We calculate the comoving volume element per redshift interval as (Hogg 1999)

$$\frac{dV}{dz} = 4\pi\, f_{\mathrm{sky}}\, \frac{c}{H_0}\, \frac{(1+z)^2\, d_{\mathrm{A}}(z)^2}{E(z)} \,, \tag{6}$$

where c is the speed of light, and d_{A} the angular diameter distance. Using N-body simulations, Jenkins et al. (2001) obtained the following fitting formula for the mass function of dark matter halos:

$$\frac{\mathrm{d}n(M,z)}{\mathrm{d}\ln\sigma^{-1}} = \frac{\bar{\rho}}{M}\, A \exp\left[-|\ln\sigma^{-1} + B|^{\epsilon}\right] \,, \tag{7}$$

where $\bar{\rho}$ is the mean comoving matter density of the Universe and A, B and ϵ are fitted parameters. Here $\sigma^2(M, z)$ is the variance of the linearly evolved density field, smoothed by a spherical top-hat filter, $W(k; M)$. In Fourier-space representation,

$$\sigma^2(M, z) = \frac{b^2(z)}{2\pi^2} \int_{0}^{\infty} k^2 P(k) W^2(k; M) \mathrm{d}k, \tag{8}$$

where k is the wave number, $P(k)$ is the power spectrum of the linear density field extrapolated to redshift zero and $b(z)$ is the growth factor of linear perturbations normalized to be 1 when $z = 0$. We calculate the power spectrum using the fitting formula obtained by Bond & Efstathiou (1984). For halo finding algorithms tied to the mean mass density, Jenkins et al. (2001) showed that the values of A, B and ϵ are almost invariant under both a broad range of cosmologies and redshift. However, these authors also showed that these parameters depend on the cluster finding algorithm. Here, we use $A = 0.316$, $B = 0.67$, $\epsilon = 3.82$ (Jenkins et al. 2001), which are appropriate for the spherical overdensity

algorithm SO($\kappa = 324$) (Davis et al. 1985; Lacey & Cole 1994), where κ is the mean overdensity of the halo with respect to the mean matter density of the Universe.

In equation (5) we have a log-normal probability distribution

$$P(L'|M) = \frac{e^{[\log_{10} L' - \log_{10} \hat{L}'(M)]^2 / 2\sigma^2}}{L' \ln(10)\sqrt{2\pi}\sigma} \,, \tag{9}$$

where $\hat{L}'(M)$ is the best fit luminosity for a given mass M, and σ is its scatter, determined from the mass-luminosity data set of Reiprich & Böhringer (2002) using the relation

$$\log_{10}\left[\frac{M\, E(z)}{h_{72}^{-1} M_{\odot}}\right] = \mathcal{A} + \alpha \log_{10}\left[\frac{L_{\mathrm{X}}(0.1 - 2.4\,\mathrm{keV})}{10^{44} h_{72}^{-2}\,\mathrm{erg\,s^{-1}}\, E(z)}\right] \,, \tag{10}$$

for which $\alpha = 0.607$ and $\mathcal{A} = \log_{10}\left[M_0/(h_{72}^{-1} M_{\odot})\right] = 14.72$, and $\sigma = 0.22$. In equation (5) we also have a Gaussian probability distribution

$$p(L|L') = \frac{e^{[L - L']^2 / 2\sigma_{\mathrm{l}}^2}}{\sqrt{2\pi}\sigma_{\mathrm{l}}} \,, \tag{11}$$

with standard deviation $\sigma_{\mathrm{l}} = (\sigma_{n_{\mathrm{ph}}}/n_{\mathrm{ph}})L'$. Here n_{ph} is the number of photons detected from a cluster in the survey and $\sigma_{n_{\mathrm{ph}}} = \sqrt{n_{\mathrm{ph}}}$ is the associated Poisson error. We assume, $n_{\mathrm{ph}} \sim 20$ at the flux limit of the survey.

3.2.2   *Temperature selection*

In order to minimize systematic scatter in the f_{gas} experiment, Allen et al. (2007) restrict their analysis to dynamically relaxed clusters with mean gas mass-weighted temperatures measured within r_{2500},[5] $kT_{2500} > 5\,\mathrm{keV}$. We impose the same temperature cut in this analysis, calculating the luminosity limit L_{i} that corresponds to this temperature limit from the relation

$$\log_{10}\left[\frac{L_{\mathrm{X}}(0.1 - 2.4\,\mathrm{keV})}{10^{44} h_{72}^{-2}\,\mathrm{erg\,s^{-1}}\, E(z)}\right] = A + B \log_{10}\left(\frac{kT_e}{\mathrm{keV}}\right) \,, \tag{12}$$

where T_e is the emission weighted X-ray temperature, which we assume scales with the mass-weighted temperature within r_{2500} as $kT_{\mathrm{e}} \sim kT_{2500}/\eta$,[6] with $\eta \sim 1.1 - 1.2$. Fitting the above relation (12) to the X-ray luminosity and temperature data of Reiprich & Böhringer (2002), we obtain $A = -1.14$ and $B = 2.50$.[7]

The limiting luminosity in equation (5) is then

$$L_{\mathrm{lim}}(z) = \min[L_{\mathrm{i}}, 4\pi F_{\mathrm{lim}} d_{\mathrm{L}}(z)^2] \,, \tag{13}$$

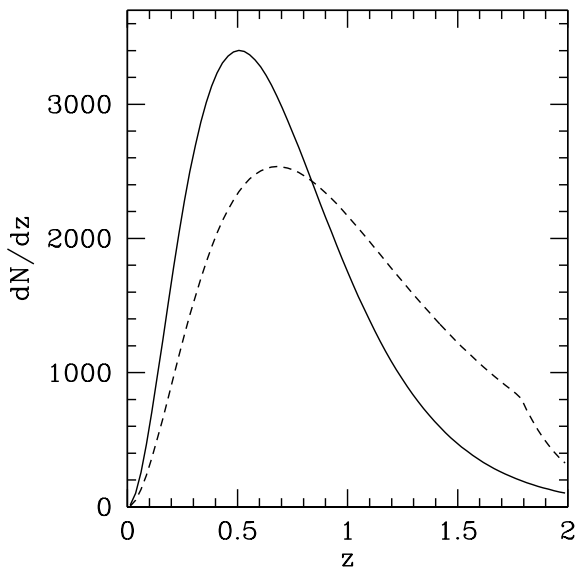with the appropriate $K-$correction applied in calculating the F_{lim} values.

Figure 1. The redshift distribution (solid curve) of clusters above the Spectrum-RG/eROSITA X-ray flux limit with mass-weighted temperatures $kT_{2500} > 5$keV. A sky coverage of ~ 50 per cent is assumed. This redshift distribution has been used to generate the mock $f_{\rm gas}$ data set. Assuming that $\sim 1/6$ of such clusters will be sufficiently relaxed for $f_{\rm gas}$ work, we obtain a final sample of ~ 500 clusters. For comparison purposes, we also show (dashed curve) the redshift distribution for the case of a fixed luminosity limit $L_{\rm X}(0.1 - 2.4\,{\rm keV}) > 4.5 \times 10^{44} h_{70}^{-2}\,{\rm erg\,s^{-1}}$ (no temperature cut) which gives a similar total number of clusters. The latter distribution has more high$-z$ clusters.

3.2.3 The redshift distribution of $f_{\rm gas}$ clusters

Table 2 summarizes the parameters describing our fiducial cosmology. For this cosmology, we have calculated the redshift distribution of galaxy clusters over the range $0 < z < 2$. Our fiducial cosmology approximately matches that used by the DETF, but includes updated values for $n_{\rm s}$ and τ to better match the WMAP three-year results (Spergel et al. 2006). We also adopt a lower value for $\sigma_8 = 0.8$, consistent with both the WMAP three-year results and the results of Mantz et al. (2007) from measurements of the X-ray luminosity function of galaxy clusters within $z < 0.7$.

Figure 1 shows the redshift distribution (solid line) for clusters detected above the Spectrum-RG/eROSITA X-ray flux limit with mass-weighted temperatures $kT_{2500} > 5$keV (emission weighted temperatures $kT_{\rm e} > 4.35\,{\rm keV}$). A sky coverage, $f_{\rm sky} \sim 0.5$ is assumed. Approximately 3000 clusters meet these criteria. Assuming that $\sim 1/6$ of these clusters will also meet the relaxation criteria based on X-ray morphology (Allen et al. 2007; Million et al. 2007), a sample

[5] r_{2500} is the radius within which the mean density is 2500 times the critical density of the Universe at the redshift of the cluster.
[6] Result based on MACS clusters spanning the redshift range $0.3 < z < 0.7$ (A. Mantz, private communication).
[7] We exclude objects from the Reiprich & Böhringer (2002) sample for which the temperature was estimated from the luminosity-temperature relation of Markevitch (1998) rather than directly measured. This leaves 88 data points in total.

of ~ 500 hot, X-ray luminous, dynamically relaxed clusters can be defined.

For comparison purposes, Figure 1 also shows (dashed curve) the redshift distribution for the case of a luminosity limit of $L_{\rm i} > 4.5 \times 10^{44} h_{70}^{-2}\,{\rm erg\,s^{-1}}$ in the $0.1 - 2.4\,{\rm keV}$ band (dashed line; no temperature cut is imposed). The effect of the X-ray flux limit on the distribution is evident towards the highest redshifts ($z \sim 1.8$) in this case.

It is clear from that figure that the temperature and luminosity cuts lead to different redshift distributions. In the case of the temperature cut (solid line), the redshift distribution peaks around $z \sim 0.5$ and relatively few clusters are found at $z > 1.5$. For the case of the luminosity cut (dashed line), the distribution peaks around $z \sim 0.7$, and has many more clusters at $z > 1$. It is important to note, however, that a redshift distribution weighted towards higher redshifts does not necessarily imply tighter constraints on dark energy. For the DETF FoM criterion, constraints around the pivot redshift are important; for the $f_{\rm gas}$ experiment $z_{\rm p} \sim 0.25$ (see Figure 5).

We generate mock $f_{\rm gas}$ measurements for 500 clusters with the redshift distribution appropriate for the case of the temperature cut [solid curve, Figure 1; in accordance with the selection criteria used for current $f_{\rm gas}$ work (Allen et al. 2007)]. For each cluster, we assign a statistical error in the $f_{\rm gas}$ measurements of ~ 5 per cent. We have also generated a set of mock measurements for the case of 250 clusters observed with $f_{\rm gas}$ measurements accurate to 3.5 per cent. This latter data set is used to study the impact on the dark energy constraints in the case that the fraction of suitably relaxed clusters is less than 1/6 at high redshifts.

We stress that the predicted redshift distribution, which peaks around $z \sim 0.5$ in the case of the temperature cut, has already been probed, at least partially, over the luminosity and temperature range of interest, by the MACS survey (Ebeling et al. 2001); MACS covers the redshift range $0.3 < z < 0.7$ to a flux limit of $F_{\rm lim} = 10^{-12}\,{\rm erg\,cm^{-2}\,s^{-1}}$ in the $0.1 - 2.4\,{\rm keV}$ band. For MACS, approximately 1/4 clusters are found to be sufficiently relaxed for $f_{\rm gas}$ work (Allen et al. 2007). Therefore, our assumption that $\sim 1/6$ clusters detected in a future X-ray survey and meeting the X-ray flux and temperature criteria will be suitably relaxed, appears reasonable. Moreover, as discussed in Section 5.1, for the case of the 250-cluster sample (i.e. assuming that only $\sim 1/12$ clusters are relaxed) and using a similar total observing time to obtain individual $f_{\rm gas}$ measurements to ~ 3.5 per cent accuracy, we obtain very similar dark energy constraints.

A final important point regards contaminating point sources: for MACS clusters, the fraction of the measured $0.1 - 2.4\,{\rm keV}$ X-ray flux arising from contaminating point sources is small, typically of order a per cent (Mantz et al. 2007; this is also the case for the hottest, $kT_{\rm e} \gtrsim 5$keV, relaxed clusters at lower redshifts.) Therefore, we do not expect our target clusters, which have comparable X-ray temperatures and luminosities, to be severely affected by contaminating point sources, especially at $z \lesssim 1$. This alleviates the instrumental requirements on the point spread function; an instrument with capabilities similar to the baseline characteristics listed in Table 1 should be capable of making significant strides in dark energy work.

Table 2. Parameter values of our fiducial cosmology, which is a flat ΛCDM cosmology.

$w_0 = -1$	$\Omega_m = 0.27$	$H_0 = 72\,\mathrm{km\,s^{-1}\,Mpc^{-1}}$
$w_a = 0$	$\Omega_b = 0.046$	$n_s = 0.95$
$\Omega_{de} = 0.73$	$\sigma_8 = 0.8$	$A_s = 2.3 \times 10^{-9}$
$\Omega_k = 0$	$b = 0.82$	$\tau = 0.09$

3.3 Follow-up SZ observations

The thermal SZ effect is a difference in the CMB spectrum caused by Compton scattering of CMB photons by hot electrons in the intracluster medium. The SZ flux measured at radio or sub-mm wavelengths can be expressed in terms of the Compton $y-$parameter. For a given cosmology, the $y-$parameter can also be predicted from the same X-ray data used to determine the f_{gas} measurements, being proportional to the integral along the line-of-sight of the product of electron density and temperature, $\int n_e T_e dl$.

We have examined the additional cosmological constraining power that can be achieved with follow-up radio/sub-mm SZ observations of our sample of 500 clusters, assuming direct SZ flux measurements accurate to 2 or 5 per cent (a level of accuracy that should be straightforward for SZ detector technology available at the time of the experiment; see Muchovej et al. 2007, and references therein). The statistical uncertainties in the predicted Compton $y-$parameters will be comparable to those associated with the f_{gas} measurements: ~ 5 per cent for the 500-cluster sample. We generate our predicted $y-$parameter data set for the redshift distribution shown in Fig. 1 (solid curve).

3.4 Mock CMB data sets

We have used the CAMB code (Lewis et al. 2000)[8] to generate auto and cross temperature and polarization angular power spectra, C_l^{TT}, C_l^{TE} and C_l^{EE}, for the fiducial, flat ΛCDM cosmology described in Table 2. We follow Lewis (2005) and Lewis et al. (2006) and assume that the temperature, T, and polarization $E-$fields are Gaussian and isotropic. We also assume that the polarization $B-$field is negligible.

Having C_l^{TT}, C_l^{TE} and C_l^{EE}, we add a simple, isotropic noise power spectrum (Cooray et al. 2000; Lewis 2005; Lewis et al. 2006)

$$N_l(\nu', \nu) = \mathcal{N}_l(\nu)\, \delta_{\nu',\nu}\, e^{b(\nu)^2 l(l+1)/8 \ln 2}, \qquad (14)$$

where $\mathcal{N}_l(\nu) = [b(\nu)\sigma(\nu)]^2$, $b(\nu) = \sqrt{8 \ln 2}\,\sigma(\nu)$ is the beam full width at half maximum (FWHM) measured in radians, and $\sigma(\nu) = (\Delta T/T)^2$ is the root mean square noise per beam-sized pixel. Assuming uncorrelated noise in the E and T fields, the covariance over realizations is (Lewis et al. 2006)

$$C_l = \begin{pmatrix} C_l^{\mathrm{TT}} + N_l^{\mathrm{TT}} & C_l^{\mathrm{TE}} \\ C_l^{\mathrm{TE}} & C_l^{\mathrm{EE}} + N_l^{\mathrm{EE}} \end{pmatrix}. \qquad (15)$$

For the channel $\nu = 143\,\mathrm{GHz}$, $\mathcal{N}_l^{\mathrm{TT}}(\nu) = \mathcal{N}_l^{\mathrm{EE}}(\nu)/4 = 2 \times 10^{-4}\,\mu\mathrm{K}^2$ and $b(\nu) = 7.1$ arcmin (Lewis et al. 2006). These values correspond to $\sigma(\nu)^{\mathrm{TT}} = 6.97\,\mu\mathrm{K}$ and $\sigma(\nu)^{\mathrm{EE}} = 9.68\,\mu\mathrm{K}$, which is roughly the sensitivity expected for PLANCK [9] after ~ 2 years (14 months) of a full sky survey (Planck 2006).

We consider two different scenarios relating to foreground CMB polarization contamination. Firstly, we examine the idealized case where such contamination can be neglected (Bond et al. 2004; Lewis 2005; Lewis et al. 2006; Planck 2006). Secondly, we consider a more conservative scenario where ~ 20 per cent of the sky is irretrievably contaminated by Galactic emission, leaving ~ 80 per cent that can be modelled as approximately foreground-free. For the second scenario, Tegmark et al. (2000) forecast that PLANCK will be able to determine the optical depth to reionization to a precision of $\sigma(\tau) \sim 0.01$, as compared to $\sigma(\tau) \sim 0.005$ for the idealized, foreground-free case (Bond et al. 2004; Lewis et al. 2006; Planck 2006). To account for the effects of polarization contamination, the DETF discarded polarization information for multipoles $l < 30$ and imposed a prior on τ to obtain $\sigma(\tau) = 0.01$. For our analysis in the case of polarization contamination, we also artificially weaken the constraints on τ to a precision of $\sigma(\tau) \sim 0.01$ by enlarging by an order of magnitude the noise at low multipoles $l < 30$ in the polarization data.

For both scenarios, we use only the data from multipoles $2 \leqslant l \leqslant 2000$. For simplicity, we adopt the zero-contamination scenario as our default CMB data set.

4 DATA ANALYSIS METHOD

4.1 Markov Chain Monte Carlo (MCMC) code

Given the dark energy model described in Section 2 and the simulated f_{gas} and CMB data sets described in Section 3, we use the Metropolis Markov Chain Monte Carlo (MCMC) algorithm implemented in the COSMOMC [10] (Lewis & Bridle 2002) package to examine posterior parameter distributions. We use a modified version of the CAMB (Lewis et al. 2000) code to calculate CMB power spectra; this accounts for the effects of dark energy perturbations for evolving dark energy equations of state (Rapetti et al. 2005) (see Section 4.5 for details). Our modified version of the COSMOMC code also incorporates the f_{gas} analysis method described by Allen et al. (2007) (see also Rapetti et al. 2005, 2007).

Our choice to forecast parameter constraints using a full MCMC analysis has some advantages over the more widely used Fisher matrix formalism (see discussions in Perotto et al. 2006; Lewis et al. 2006). Firstly, the shape of the mean log likelihood [see equation (22)] (Lewis et al. 2006) in the MCMC analysis encapsulates all of the relevant degeneracies between parameters, which is crucial for non-Gaussian distributions. Secondly, the fact that our forecasts are made using the same COSMOMC analysis code used to analyze current data (Allen et al. 2007) ensures consistency between present and future constraints. Finally, the MCMC method allows

---

[8] http://camb.info/

[9] http://www.rssd.esa.int/index.php?project=Planck
[10] http://cosmologist.info/cosmomc/

us to easily and efficiently introduce priors and allowances and thereby study the effects of systematic uncertainties.

4.2 X-ray gas mass fraction analysis

4.2.1 The f_{gas} method

The X-ray gas mass fraction, f_{gas}, is defined as the ratio of the X-ray emitting gas mass to the total mass of a cluster. This quantity can be determined from the observed X-ray surface brightness and the deprojected, spectrally-determined gas temperature profile, under the assumptions of spherical symmetry and hydrostatic equilibrium. To ensure that these assumptions are as accurate as possible, it is essential to limit the f_{gas} analysis to the hottest, most X-ray luminous, dynamically relaxed clusters available [Section 3.1; for a detailed discussion of the method and current measurements see Allen et al. (2007) and references therein.]

In order to study dark energy, Allen et al. (2007) use f_{gas} measurements for a sample of 42 hot ($kT_{2500} > 5$keV), X-ray luminous, dynamically relaxed clusters. The f_{gas} measurements are made at an angle $\theta_{2500}^{\Lambda CDM}$ for each cluster, corresponding to r_{2500} for a reference flat ΛCDM cosmology (with $\Omega_m = 0.3$ and $H_0 = 70 \, \mathrm{km \, s^{-1} \, Mpc^{-1}}$). The f_{gas} measurements in the reference cosmology $f_{gas}^{\Lambda CDM}$ are related to the true values f_{gas}^{true} as

$$f_{gas}^{\Lambda CDM}(z; \theta_{2500}^{\Lambda CDM}) = f_{gas}^{true}(z; \theta_{2500}^{\Lambda CDM}) \left(\frac{d_A^{\Lambda CDM}}{d_A^{true}} \right)^{3/2} . \quad (16)$$

Current hydrodynamical simulations (Eke et al. 1998; Nagai et al. 2007; Crain et al. 2007) suggest that f_{gas}^{true} is likely to be approximately constant in redshift. Thus (Allen et al. 2007),

$$f_{gas}^{true}(z; \theta_{2500}^{true}) = \left(\frac{\Omega_b}{\Omega_m} \right) \left(\frac{b_0}{1 + s_0} \right) , \quad (17)$$

where $s_0 = 0.16 h_{70}^{0.5}$ (Lin & Mohr 2004) is the observed ratio of the mass in stars (both in galaxies and intracluster light) to the X-ray emitting gas mass, and $b_0 = 0.82$ (Eke et al. 1998) is the depletion factor for the baryon fraction in clusters with respect to the cosmic mean value.

As discussed by Allen et al. (2007), an angular correction factor is also required to account for the fact that $f_{gas}^{true}(z; \theta_{2500}^{true})$ is not exactly equal to $f_{gas}^{true}(z; \theta_{2500}^{\Lambda CDM})$. Observations of large, relaxed clusters show that for the radial range of interest, $0.7 < r/r_{2500} < 1.2$, the $f_{gas}(r)$ profiles can be fit by a shallow power-law model with slope $\eta = 0.214 \pm 0.022$.[11] Thus, we have

$$f_{gas}^{true}(z; \theta_{2500}^{\Lambda CDM}) = f_{gas}^{true}(z; \theta_{2500}^{true}) \left(\frac{\theta_{2500}^{\Lambda CDM}}{\theta_{2500}^{true}} \right)^{\eta} , \quad (18)$$

where $\theta_{2500} = r_{2500}/d_A$, and

$$\left(\frac{\theta_{2500}^{\Lambda CDM}}{\theta_{2500}^{true}} \right)^{\eta} = \left(\frac{[H(z) \, d_A(z)]^{true}}{[H(z) \, d_A(z)]^{\Lambda CDM}} \right)^{\eta} . \quad (19)$$

This correction factor is small and can be neglected for most analyses of current data, although its inclusion leads to slightly tighter constraints on dark energy (Allen et al. 2007). However, for future experiments of the precision being considered here, the inclusion of the angular correction term becomes important.

4.2.2 Allowances for systematic uncertainties

Following Allen et al. (2007), we modify equation (17) to account for systematic uncertainties in the f_{gas} analysis:

$$f_{gas}^{true}(z; \theta_{2500}^{true}) = \gamma \, K \left(\frac{\Omega_b}{\Omega_m} \right) \left(\frac{b(z)}{1 + s(z)} \right) . \quad (20)$$

Here γ allows for departures from the assumption of hydrostatic equilibrium, due to non-thermal pressure support; K is a normalization uncertainty relating to instrumental calibration and certain modelling issues; $b(z) = b_0(1 + \alpha_b z + \beta_b z^2)$ accounts for uncertainties in the cluster depletion factor, both in the normalization, b_0, and possible linear, α_b, and quadratic, β_b, evolution with redshift; $s(z) = s_0(1 + \alpha_s z + \beta_s z^2)$ accounts for uncertainties in the stellar mass fraction.[12]

Using hydrodynamic N-body simulations Nagai et al. (2007) show that for large, relaxed clusters, non-thermal pressure support is unlikely to exceed 8 per cent. Furthermore if, as suggested by some current X-ray data (Fabian et al. 2003, 2005; Reynolds et al. 2005), the gas viscosity is higher than included in current simulations, then non-thermal pressure support could be even lower. Based on these findings, we adopt by default a uniform prior such that non-thermal pressure support lies in the range $0 - 8$ per cent (although a more pessimistic range of $0 - 16$ per cent is also considered). Since the use of asymmetric prior would bias the analysis, levering Ω_m above the fiducial value, we employ an equivalent, rescaled symmetric prior such that $1 - (a/2) < \gamma < 1 + (a/2)$, where $a = |1 - 1.08|/1.04$.

The depletion parameter, b_0, reflects the thermodynamic history of the X-ray emitting cluster gas. Using adiabatic simulations of hot, massive clusters of comparable size to the real clusters to be used in the f_{gas} experiment, Eke et al. (1998) (see also Allen et al. 2004; Nagai et al. 2007; Crain et al. 2007) obtained $b_0 = 0.82 \pm 0.03$ at the radius of the measurements r_{2500} ($\sim 0.25 r_{vir}$) and found no evidence for redshift evolution: $\alpha_b = 0.00 \pm 0.03$ for measurements made at $r \sim 0.5 r_{vir}$, spanning the redshift range $0 < z < 1$. As discussed by Allen et al. (2007), however, systematic uncertainties are associated with current predictions for $b(z)$, due to limitations in the accuracy for the physical approximations employed in the simulations. Estimating the residual uncertainties in the prediction of $b(z)$ that will be appropriate at the time of a future f_{gas} data set ($\sim 2015 - 2020$) is difficult. We have chosen to use a range of values that extend from optimistic to pessimistic scenarios (see Table 3).

Current optical and near infrared data for low-to-intermediate redshift clusters give $s_0 = 0.16 h_{70}^{-0.5}$ (Fukugita

---

[11] Note that even using two very different reference cosmologies such as SCDM ($\Omega_m = 1$, $H_0 = 50 \, \mathrm{km \, s^{-1} \, Mpc^{-1}}$) and ΛCDM ($\Omega_m = 0.3$, $H_0 = 70 \, \mathrm{km \, s^{-1} \, Mpc^{-1}}$), Allen et al. (2007) obtained similar values for η around r_{2500}.

[12] Working with current data, Allen et al. (2007) use only the linear order of the redshift expansions for their systematic allowances i.e. α_b and α_s.

Table 3. Systematic allowances incorporated in the f_{gas} and XSZ experiments.

Cluster	Parameter	Allowance (optimistic/standard/pessimistic)	Type
f_{gas} EXPERIMENT			
Calibration/Modelling	K	$1.0 \pm 0.02/\pm 0.05/\pm 0.10$	Gaussian
Non-thermal pressure	γ	$0.96 < \gamma < 1.04/0.92 < \gamma < 1.08$	uniform
Gas depletion: norm.	b_0	$0.82 \times (1 \pm 0.02/\pm 0.05/\pm 0.10)$	uniform
Gas depletion: evol. (linear)	α_{b}	$\pm 0.02/\pm 0.05/\pm 0.10$	uniform
Gas depletion: evol. (quadratic)	β_{b}	$\pm 0.02/\pm 0.05/\pm 0.10$	uniform
Stellar mass: norm.	s_0	$0.16 \times (1 \pm 0.02/\pm 0.05/\pm 0.10)$	Gaussian
Stellar mass: evol. (linear)	α_{s}	$\pm 0.02/\pm 0.05/\pm 0.10$	uniform
Stellar mass: evol. (quadratic)	β_{s}	$\pm 0.02/\pm 0.05/\pm 0.10$	uniform
XSZ EXPERIMENT			
Calibration/Modelling	k_0	$1.0 \pm 0.02/\pm 0.05$	Gaussian
evolution (linear)	α_{k}	$\pm 0.02/\pm 0.05/\pm 0.10$	uniform

et al. 1998; Lin & Mohr 2004). Although, at present, the constraints on $s(z)$ for clusters at $z \gtrsim 0.5$ are sparse, we expect the form of $s(z)$ to be relatively well understood by the time of the f_{gas} experiment.

In order to keep the interpretation of our results simple, we present results for three sets of systematic allowances: for the parameters, $K, b_0, \alpha_{\text{b}}, \beta_{\text{b}}, s_0, \alpha_{\text{s}}, \beta_{\text{s}}$, we employ allowances of either ± 2 per cent (optimistic), ± 5 per cent (standard), or ± 10 per cent (pessimistic). In all cases, we employ uniform priors with the exception of K and s_0, for which Gaussian priors are more appropriate and therefore used. As noted above, a uniform allowance of ± 4 per cent on γ, is included by default, although the effects of doubling the uncertainty in this parameter are also examined. We stress that whether $\gamma = 1$ precisely, or $\alpha_{\text{b}}, \alpha_{\text{s}}$ etc are precisely zero, is not of primary importance to a future analysis: if known, the exact values can be incorporated into the default model. It is the uncertainties in the values that affect the accuracy and precision of the dark energy constraints.

4.3 Analysis of the SZ data: the XSZ experiment

For the true, underlying cosmology, the measurement of the Compton $y-$parameter from both the X-ray and SZ data should match (e.g. Molnar et al. 2002; Schmidt et al. 2004; Bonamente et al. 2006). For a given cosmology the y-parameter predicted by X-ray data depends on the angular diameter distance to the cluster $d_{\text{A}}^{0.5}$, whereas the observed SZ flux at radio or sub-mm wavelengths is independent of the cosmology assumed. Combining the $y-$parameter results, we can measure the distances to the clusters as a function of redshift and, therefore, constrain dark energy.

$$y^{\Lambda\text{CDM}} = y^{\text{SZobs}} k(z) \left(\frac{d_{\text{A}}^{\Lambda\text{CDM}}}{d_{\text{A}}^{\text{true}}} \right)^{1/2} . \qquad (21)$$

Here $y^{\Lambda\text{CDM}}$ is the X-ray measurement of the y-parameter for the reference cosmology and y^{SZobs} is the radio/sub-

mm observation.[13] Following a similar approach to that adopted with the f_{gas} data, we incorporate systematic allowances into equation (21): $k(z) = k_0(1 + \alpha_{\text{k}}z)$ accounts for the combined systematic uncertainties in the X-ray and SZ data $y-$parameter measurements due to calibration, geometric effects, gas clumping, etc., and their evolution. We employ Gaussian priors on k_0 of size 2 (optimistic) or 5 (standard/pessimistic) per cent and uniform priors on α_{k} of size 2 (optimistic), 5 (standard) or 10 (pessimistic) per cent.

We note that the best clusters to observe for the XSZ experiment are the same systems used for the f_{gas} experiment: the largest, most dynamically relaxed clusters. These are the clusters for which the SZ signals are strongest and for which systematic uncertainties associated with geometry and thermodynamic structure are minimized. Note also that no additional X-ray observations are required to carry out the XSZ experiment, once the f_{gas} data are in hand.

4.4 Incorporating the CMB data

In addition to the dark energy model parameters and the f_{gas} parameters discussed in Section 4.2, we vary the following eight CMB-related parameters in the MCMC analysis: the mean physical baryon density $\Omega_{\text{b}}h^2$, the mean physical cold dark matter density $\Omega_{\text{dm}}h^2$, the (approximate) ratio of the sound horizon at last scattering to the angular diameter distance θ_{s} (Kosowsky et al. 2002), the optical depth to reionization τ (assumed to occur in a sharp transition), the mean curvature density of the Universe Ω_{k}, the scalar adiabatic spectral index n_{s}, and the scalar adiabatic amplitude A_{s} at $k = 0.05 \,\text{Mpc}^{-1}$. We employ a uniform prior on $\ln(A_{\text{s}})$. The combination of θ_{s} and $\ln(A_{\text{s}})$ as parameters, rather than H_0 and A_{s}, leads to a more Gaussian probability density distribution which, in turn, aids sampling (Kosowsky et al. 2002; Lewis et al. 2006).

The degeneracies between dark energy model parameters and Ω_{k} are of particular importance in the analysis

---

[13] The limitations of existing SZ data have to date restricted the XSZ experiment to measurements of the Hubble constant (e.g. Bonamente et al. 2006, and references therein).
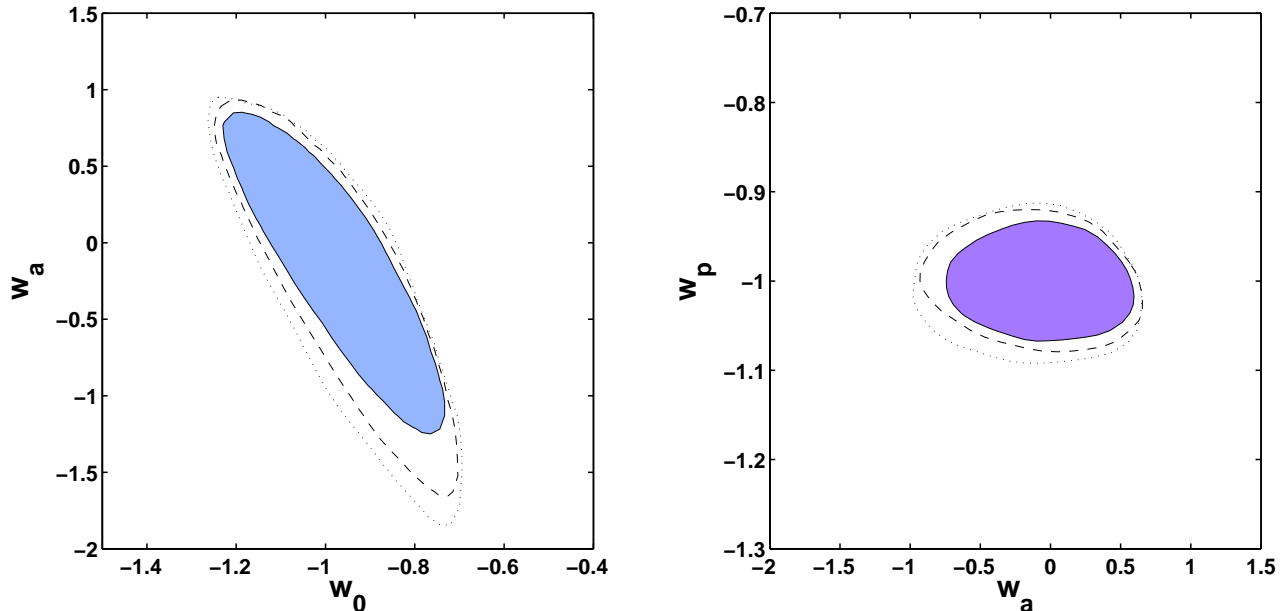
Figure 2. (Left panel) The 95 per cent confidence contours in the $w_0 - w_a$ for the default dark energy model using the optimistic (2 per cent; blue, solid contour), standard (5 per cent; dashed contour) and pessimistic (10 per cent; dotted contour) allowances. (Right panel) The 68 per cent confidence contours in the $w_a - w_p$ plane for the default dark energy model using the optimistic (2 per cent; purple, solid contour), standard (5 per cent; dashed contour) and pessimistic (10 per cent; dotted contour) allowances. The marginalized 1σ confidence intervals on w_a and w_p are used to calculate the FoM. The figure confirms that w_a and w_p are not strongly correlated, as assumed in the definition of the FoM (Section 2).

(Rapetti et al. 2005; Clarkson et al. 2007).[14] For their forecasts, the DETF include PLANCK priors in their Fisher matrix analysis, approximating the role of future CMB constraints as well as the degeneracies between the dark energy parameters and Ω_k. Here, we account fully for the degeneracies between parameters, and the complementarity of the data sets.

Given the vector, ϵ of CMB-related parameters, we sample the exponential of the following mean logarithmic likelihood (Lewis 2005; Lewis et al. 2006)

$$< \ln P(\epsilon|\epsilon_0) >= -\frac{1}{2}[Tr(C_1(\epsilon_0)C_1(\epsilon)^{-1}) + \ln |C_1(\epsilon)|], \quad (22)$$

where ϵ_0 is the vector formed by the corresponding fiducial values of Table 2. Note that where the posterior is non-Gaussian, the marginalized constraints on individual parameters need not peak exactly at the fiducial values, although for all cases considered here the differences are very small.

4.5 Dark energy clustering

For a dark energy model with a constant equation of state, w, Weller & Lewis (2003) and Bean & Dore (2004) showed that dark energy clustering can have a non-negligible impact on the constraints, driven primarily by the effect of

---

[14] Allen et al. (2004, 2007) and Rapetti et al. (2005) showed that the combination of f_{gas} plus CMB data allows one to drop both the assumption of flatness and the priors on $\Omega_b h^2$ and h that would otherwise be required for the f_{gas} analysis. The f_{gas}+CMB data combination also alleviates other important parameter degeneracies e.g. between $\Omega_b h^2$, n_s and τ.

such perturbations on the Integrated Sachs-Wolfe (ISW) effect. Spergel et al. (2006) showed that accounting for dark energy clustering has a large effect on current dark energy constraints derived from CMB data alone. Since, for constant$-w$ models, combining the CMB data with e.g. distance measurements from type Ia supernovae or X-ray galaxy clusters leads to tight constraints on w and a result consistent with a cosmological constant ($w = -1$, for which no dark energy clustering occurs), the importance of accounting for dark energy perturbations is reduced (Weller & Lewis 2003; Rapetti et al. 2005; Spergel et al. 2006). However, when one considers more general models in which w evolves, Rapetti et al. (2005) showed that even with the best current data combinations, accounting for the effects of dark energy perturbations is important: the constraints on $w(a)$ increase by a factor of ~ 2 with respect to the case where dark energy clustering is (wrongly) ignored.

For our analysis, we assume that dark energy is an imperfect fluid where dissipative processes generate entropy perturbations. As suggested by quintessence scenarios, we assume a constant, general (non-adiabatic) sound speed $\hat{c}_s^2 = 1$ in the comoving frame of the fluid (denoted by the circumflex $\hat{}$). This is the only frame for which the general sound speed is gauge invariant (Bean & Dore 2004). Following Weller & Lewis (2003) and Bean & Dore (2004), Rapetti et al. (2005) extended the dark energy perturbation equations to account for an evolving dark energy equation of state, $w(a)$. As in Rapetti et al. (2005) we calculate the density, δ, and velocity, v, perturbation equations (Ma & Bertschinger 1995) in the synchronous gauge

$$\dot{\delta} = -3\mathcal{H}(\hat{c}_s^2 - w)\hat{\delta} - (1 + w)(kv + 3\dot{A}) + \mathcal{E}(\dot{w}) \quad (23)$$

Table 4. The 1σ uncertainties on the dark energy parameters and FoM. Systematic allowances of 2 per cent (optimistic), 5 per cent (standard) or 10 per cent (pessimistic) have been used. Results are presented for the default model and for six other cases, described in the text.

Allowances	Model	$\hat{\sigma}(w_0)$	$\hat{\sigma}(\Omega_{\mathrm{de}})$	$\hat{\sigma}(w_{\mathrm{p}})$	$\hat{\sigma}(w_{\mathrm{a}})$	$[\hat{\sigma}(w_{\mathrm{p}}) \times \hat{\sigma}(w_{\mathrm{a}})]^{-1}$	(percentage)
	Run			Dark energy parameters		FoM	ΔFoM/FoM
2%	Default	0.100	0.009	0.044	0.43	52.4	–
2%	DE clustering	0.109	0.009	0.044	0.48	46.8	-10.7%
2%	CMB conservative	0.108	0.009	0.045	0.49	44.6	-14.8%
2%	Quadratic	0.116	0.009	0.047	0.50	43.3	-17.4%
2%	250-sample	0.110	0.009	0.047	0.47	45.5	-13.1%
2%	Double γ	0.103	0.012	0.049	0.45	44.6	-14.9%
2%	Adding XSZ	0.097	0.009	0.043	0.43	54.6	+4.2%
5%	Default	0.108	0.015	0.052	0.51	37.4	–
5%	DE clustering	0.119	0.015	0.051	0.59	33.4	-10.7%
5%	CMB conservative	0.115	0.016	0.053	0.58	32.6	-12.8%
5%	Quadratic	0.126	0.014	0.069	0.51	28.7	-23.3%
5%	250-sample	0.119	0.016	0.057	0.55	31.6	-15.4%
5%	Double γ	0.108	0.017	0.054	0.51	36.5	-2.3%
5%	Adding XSZ	0.102	0.014	0.050	0.49	41.2	+10.2%
10%	Default	0.110	0.023	0.058	0.53	32.6	–
10%	DE clustering	0.132	0.022	0.054	0.66	27.9	-14.4%
10%	CMB conservative	0.118	0.026	0.063	0.60	26.6	-18.4%
10%	Quadratic	0.141	0.023	0.102	0.55	17.9	-45.1%
10%	250-sample	0.119	0.024	0.062	0.56	29.0	-11.3%
10%	Double γ	0.110	0.024	0.059	0.53	31.8	-2.5%
10%	Adding XSZ	0.106	0.020	0.055	0.52	34.8	+6.5%

$$\dot{v} \;=\; -\mathcal{H}(1 - 3\hat{c}_{\mathrm{s}}^2)v + \frac{k\hat{c}_{\mathrm{s}}^2\delta}{1 + w} \,, \tag{24}$$

where both derivatives, denoted by dots, and the Hubble parameter, $\mathcal{H}$, are with respect to conformal time. $\mathcal{A} = \delta a/a$ is the metric perturbation and $\hat{\delta}$ is the density perturbation in the comoving frame of the dark energy fluid. The density perturbation, $\hat{\delta}$, can be recast into the CDM comoving frame density and velocity perturbations, δ and v, using the relation given by Kodama & Sasaki (1984), $\hat{\delta} = \delta + 3\mathcal{H}(1+w)v/k$. Using this relation in equation (23), we recover the perturbation equations of Weller & Lewis (2003); Bean & Dore (2004) except that here w depends on the scale factor a and introduces a new source term, $\mathcal{E}(\dot{w}) = 3\mathcal{H}\dot{w}v/k$, in the density perturbation equation. Note that this term depends on the derivative of the equation of state, $\dot{w}$. Equation (24) does not have a new term.

As discussed by Vikman (2005); Caldwell & Doran (2005) a single classical scalar field cannot evolve from a quintessence-like, $w > -1$, to phantom-like, $w < -1$, behavior. However, Onemli & Woodard (2002, 2004) proposed a single scalar field model where a super-accelerated phase ($w < -1$) of the cosmic expansion can be achieved via quantum effects. Later, Kahya & Onemli (2006) showed that this model is stable. Alternatively, Feng et al. (2005); Guo et al. (2005); Hu (2005); Zhao et al. (2005) suggested the so-called quintom model: in this model, the effective equation of state of two combined scalar fields, one with $w > -1$ and the other with $w < -1$, can cross the cosmological-constant boundary, $w = -1$, as it evolves in time. Other models that allow $w(a)$ to cross this boundary have also been proposed. However, for practical purposes, using an effective, evolving dark energy equation of state produces a well-known divergence in equation (24) when $w(a) = -1$. This divergence can be avoided (Huey 2004; Caldwell & Doran 2005) by imposing $\dot{\hat{\delta}} = 0$ and $\dot{v} = 0$ within the logarithmic singularity region, $w = -1 + |\epsilon|$, where ϵ is infinitesimally small. Inaccuracies in this approximation have a negligible impact on the resulting CMB power spectra (Rapetti et al. 2005; Xia et al. 2006, 2007).

In what follows, we present results for cases where dark energy clustering is either accounted for or ignored in the CMB analysis (Section 5.3). Dark energy clustering does not have a significant impact on the f_{gas} analysis.
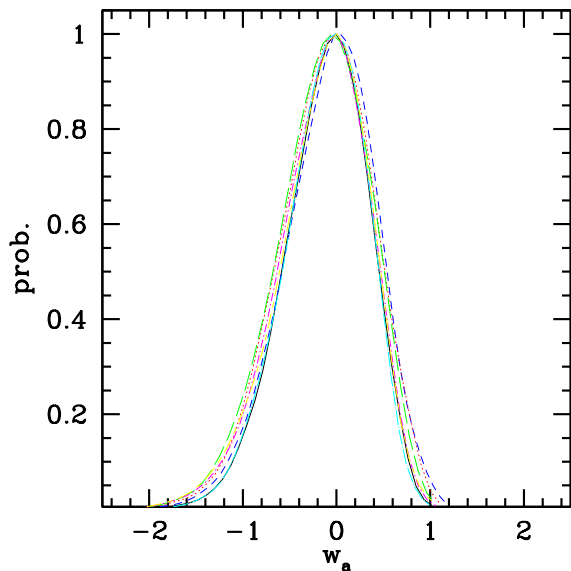
Figure 3. Posterior probability distributions for w_a for the cases described in Table 4: default scenario (black, solid line), with dark energy clustering (blue, long dashed line), conservative CMB data (red, dotted line), including quadratic evolution allowances (green, long dashed line), using the 250-cluster sample with 3.5 per cent measurement errors (magenta, dot-dashed line), doubling the systematic allowance on γ (yellow, long-short dashed) and adding the XSZ experiment (cyan, long dot-dashed line). The (optimistic) 2 per cent systematic allowances are used in every case.

5 RESULTS

As described in Section 2, to enable a direct comparison with the predicted dark energy constraints for other planned experiments, we parameterize our results in terms of the DETF FoM. We present results for a fiducial f_{gas}+CMB data set, incorporating the statistical uncertainties and allowances described above, but with zero scatter about the fiducial curve. The absence of scatter ensures that the peaks of the posterior probability distributions occur at the expected values. The use of a zero-scatter realization does not affect the FoM. We have explicitly confirmed this by comparing the FoM for the fiducial realization to a series of simulations in which scatter about the fiducial curve, at the appropriate level for the statistical measurement errors, was included.

5.1 Constraints on the FoM

In the first case, we determine constraints for a 'default' analysis: this involves f_{gas} data for 500 clusters measured to 5 per cent accuracy and CMB data with negligible foreground contamination. We ignore the effects of dark energy clustering (as do the DETF) and allow linear evolution in $b(z)$ and $s(z)$. No follow-up SZ data are included.

The constraints from the default analysis are shown in Figures 2, 4, and 5. The left panel of Figure 2 shows the well-known degeneracy between w_0 and w_a. The right panel of that figure shows the constraints in the $w_a - w_p$ plane. The results from the MCMC analysis confirm that w_p and w_a are approximately uncorrelated, which facilitates the simple

calculation of the FoM=$[\hat{\sigma}(w_p) \times \hat{\sigma}(w_a)]^{-1}$ a described in Section 2.

Table 4 summarizes the results on w_0, w_a, w_p, Ω_{de} and the FoM for the default analysis and 2, 5 or 10 per cent systematic allowances. Also included in the table are results for five further slightly modified, interesting scenarios: for the case where we include dark energy clustering (Section 4.5); for the case where we use the more conservative CMB data set (Section 3.4); for the case where we allow quadratic redshift evolution in the gas depletion factor, β_b, and the stellar fraction, β_s (Section 4.2.2); for the case we use the 250-cluster f_{gas} data set with 3.5 per cent measurement errors; for the case where we double the systematic allowance on γ; and for the case where we include extra information from the XSZ experiment (Section 4.3). For each of these scenarios, we list results for 2 per cent (optimistic), 5 per cent (standard) and 10 per cent (pessimistic) allowances.

Interestingly, we see that constraints on dark energy are similar for most cases of interest (this is also shown graphically in Figure 3). With the optimistic, 2 per cent systematic allowances, a FOM in the range $43-55$ is obtained. For the standard, 5 per cent systematic tolerances, the FOM lies in the range $29-41$. Even with the pessimistic 10 per cent systematic allowances, we obtain a FoM in the range $18-35$.

The final column of Table 4 summarizes the percentage differences in the FoM with respect to the default model for each case of interest. We see that the greatest impact on the FoM occurs by allowing quadratic evolution in the systematic allowances; in this case we observe a ~ 20 per cent reduction in the FoM with respect to the default model for the optimistic and standard allowances, and ~ 45 per cent for the pessimistic, 10 per cent allowances. Using the standard, 5 per cent allowances, we see that accounting for dark energy clustering has only a small effect (~ 10 per cent); the inclusion of the XSZ data only leads to a modest improvement in the FoM (~ 10 per cent). Doubling the uncertainty on γ does not have a major effect on the results.

5.2 Comparison with DETF results

Comparing our results on the FoM with those reported by the DETF (page 77 of the DETF report; Albrecht et al. 2006), we find that the f_{gas} experiment [15] has similar dark energy constraining power to other leading, future (DETF stage IV) ground or space-based experiments.

Figure 4 shows the 95 per cent confidence constraints in the $\Omega_{de} - w_p$ plane for the default model and optimistic (2 per cent), standard (5 per cent) and pessimistic (10 per cent) allowances. The size of this confidence region is proportional to the FoM. The DETF (Albrecht et al. 2006) present similar figures, with the same axis scaling, for the other, future dark energy experiments. The comparable constraining power and complementary nature of the f_{gas} and other experiments can (at least in part) be seen by comparing these figures. In particular, the power of the f_{gas}(+Planck) experiment in constraining Ω_{de} is clearly evident.

---

[15] The f_{gas} experiment described here would fall under the category of stage IV experiments, as defined by the DETF.
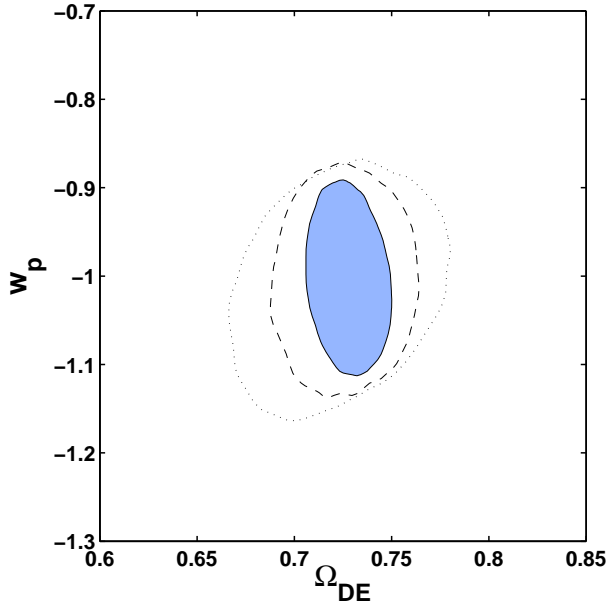
Figure 4. The 95 per cent confidence contours in the $\Omega_{\mathrm{de}} - w_{\mathrm{p}}$ plane for the default dark energy model and optimistic (2 per cent; blue, solid contour), standard (5 per cent; dashed contour) and pessimistic (10 per cent; dotted contour) allowances. The axes are scaled to cover the same region as the figures presented by the DETF.
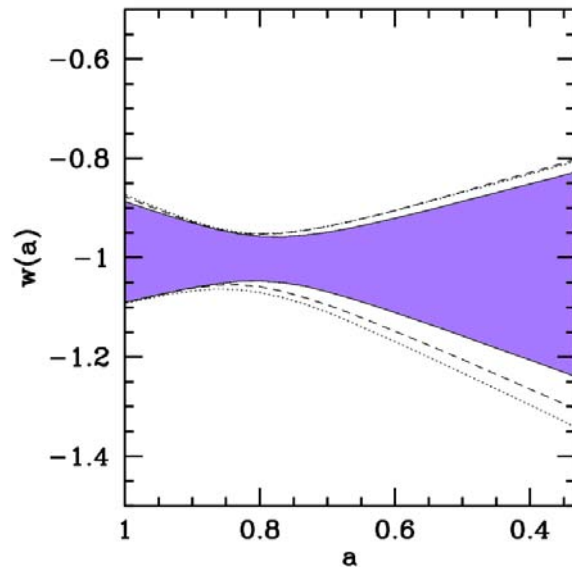

Figure 5. The 1σ confidence constraints on the evolution of the dark energy equation of state as a function of scale factor $w(a)$. Results are shown for the default model (Table 1) using the optimistic (2 per cent; shaded, purple region), standard (5 per cent; dashed line) and pessimistic (10 per cent; dotted line) systematic allowances. The tightest constraints on $w(a)$ occur at the pivot scale factor, $a_{\mathrm{p}} \sim 0.8$ ($z_{\mathrm{p}} \sim 0.25$).

5.3   The evolution of dark energy

Figure 5 shows the evolution of the dark energy equation of state as a function of scale factor, $w(a)$. The pivot scale factor, a_{p}, is the scale factor at which we obtain the tightest constraint on w [that measurement being $\sigma(w_{\mathrm{p}})$]. As shown in Figure 5, for the f_{gas} experiment we measure a pivot scale factor of $a_{\mathrm{p}} \sim 0.8$, which corresponds to a pivot redshift $z_{\mathrm{p}} \sim 0.25$. Interestingly, these values lie between the pivot scale factors/redshifts reported by the DETF for SNIa experiments ($a_{\mathrm{p}} \sim 0.93/z_{\mathrm{p}} \sim 0.075$) and galaxy cluster number counts, weak lensing and BAO experiments ($a_{\mathrm{p}} \sim 0.65/z_{\mathrm{p}} \sim 0.54$). Pinning down the evolution of w over a wide redshift range will be a crucial for unraveling the nature of dark energy. Our results argue that a combination of f_{gas}, CMB, BAO, SNIa, weak lensing and galaxy cluster number count experiments is likely to prove powerful in this regard.

5.4   The CMB data and early dark energy

The acoustic scale at last scattering, l_{a}, is tightly constrained by CMB data (Page et al. 2003) and is highly sensitive to the amount of dark energy at recombination. l_{a} changes drastically if the early dark energy density exceeds the matter plus radiation density (Wright 2007). CMB constraints on l_{a} provide a strong constraint on dark energy parameters at early times (Doran & Lilley 2002), defining a well-known boundary in the $w_0 - w_{\mathrm{a}}$ plane (Rapetti et al. 2005; Upadhye et al. 2005; Wright 2007).[16] At late times, for our experi-

ment, dark energy is constrained primarily by the f_{gas} data, with a small contribution from the Integrated Sachs-Wolfe (ISW) effect in the CMB.

A simple exercise provides further insight into how the CMB data help in constraining dark energy. For this, we re-examine the constraints in the $w_0 - w_{\mathrm{a}}$ plane obtained from the f_{gas}+CMB data; the 68 and 95 per cent confidence contours for the default model with 5 per cent allowances are shown (dashed curves) in Figure 6. The combination of f_{gas}+CMB data provides tight constraints on $\Omega_{\mathrm{b}}h^2$, $\Omega_{\mathrm{dm}}h^2$ and l_{a} (driven primarily by the CMB data), and on h (driven by the combination of both data sets). Using these constraints as priors, we examine the constraints in the $w_0 - w_{\mathrm{a}}$ plane that can be obtained from the f_{gas} data alone: the results are shown as the red, solid curves in Figure 6. We see that the priors encompass some of the CMB constraining power, in particular in defining the characteristic upper boundary in the $w_0 - w_{\mathrm{a}}$ plane. However, they do not contain the full information on e.g. the covariance of $\Omega_{\mathrm{b}}h^2$, $\Omega_{\mathrm{dm}}h^2$ and h (Rapetti et al. 2005; Wright 2007) which is also important in constraining dark energy at later times.

We note that the prior on l_{a} provides a tight constraint on the curvature. The blue dotted curves in Figure 6 show the constraints obtained from the f_{gas} data alone, using only the priors on $\Omega_{\mathrm{b}}h^2$ and h and assuming flatness.

---

[16] The presence of the boundary in the $w_0 - w_{\mathrm{a}}$ plane (Rapetti et al. 2005; Upadhye et al. 2005; Wright 2007) make it important

to consider, as is the case here, simulations that account fully for measurement uncertainties but which do not scatter about the fiducial curve. Otherwise, scatter towards the CMB boundary would increase the FoM and scatter away would decrease it, complicating the interpretation of results.
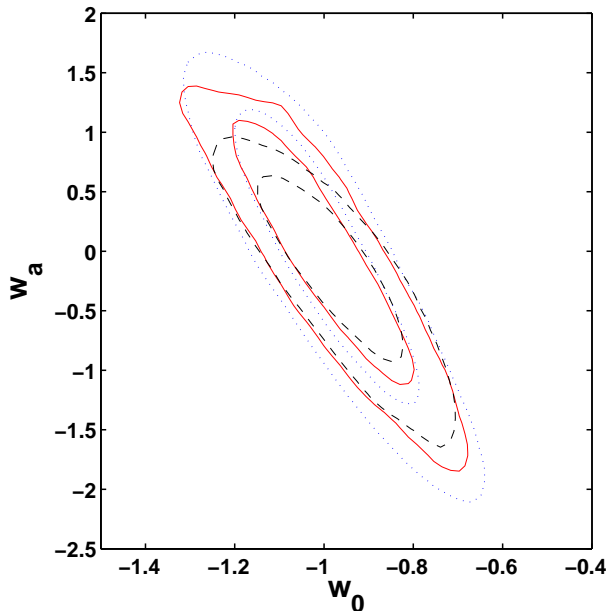
Figure 6. The 68 and 95 per cent confidence contours in the $w_0 - w_a$ plane determined from the f_{gas}+CMB data (black, dashed contours) using the default dark energy model and 5 per cent systematic allowances. The solid red lines show the constraints obtained from the f_{gas} data alone, using priors on $\Omega_b h^2$, $\Omega_{dm} h^2$, l_a and h, as described in the text (Section 5.4). The blue, dotted lines show the constraints from the f_{gas} alone using priors on $\Omega_b h^2$ and h and assuming flatness. The figure shows how the CMB data contribute in constraining dark energy, especially at early times.

5.5 The importance of the XSZ experiment

The XSZ technique provides a complementary and independent experiment to measure dark energy. Although the inclusion of constraints from the XSZ experiment leads to only modest formal improvements in the FoM with respect to the results for the f_{gas}+CMB data (Table 4; as can be expected given the relatively weak dependence on dark energy in equation 21), it is important to note that the XSZ experiment relies on different assumptions and has different systematic uncertainties. In particular, the XSZ experiment is independent of assumptions regarding hydrostatic equilibrium, the depletion factor, and the stellar mass fraction. Thus, the combination of data from the f_{gas} and XSZ techniques can help to ensure robustness in the results. In principle, the inclusion of XSZ data can also allow some of the priors in the f_{gas} experiment to be relaxed.

6 CONCLUSIONS

We have examined the ability of a future X-ray observatory, with capabilities similar to those planned for Constellation-X, to constrain dark energy via the f_{gas} experiment. We find that f_{gas} measurements for a sample of 500 hot ($kT_{2500} \gtrsim$ 5keV), X-ray bright, dynamically relaxed clusters, with a precision of ~ 5 per cent, can be used to constrain dark energy with a FoM of $20-50$. These constraints are comparable to those predicted by the DETF (Albrecht et al. 2006)

for other leading, planned (DETF Stage IV) dark energy experiments.

As discussed in the text, a future f_{gas} experiment will need to be preceded by a large X-ray or SZ cluster survey that will find hot, X-ray luminous clusters out to high redshifts. A survey such as that planned with the Spectrum-RG/eROSITA mission should find several thousand such clusters. Short 'snapshot' follow-up observations of the clusters with a new, large X-ray observatory should be able to identify a sample of ~ 500 suitable systems for f_{gas} work. Attaining a precision of ~ 5 per cent with individual f_{gas} measurements should be straightforward for an observatory with characteristics similar to Constellation-X, requiring exposure times of ~ 20ks. We note that the population of galaxy clusters in the redshift, temperature and X-ray luminosity range of interest has already been partially probed by the MACS survey (Ebeling et al. 2001); Chandra observations of MACS clusters are used extensively in current f_{gas} studies (Allen et al. 2004; LaRoque et al. 2006; Allen et al. 2007). The low-level of X-ray flux contamination from point sources observed in MACS clusters also alleviates the requirements on the instrumental PSF for dark energy work via the f_{gas} method.

In determining the predicted dark energy constraints, we have employed the same MCMC method used to analyze current data. The MCMC method encapsulates all of the relevant degeneracies between parameters and allows one to easily and efficiently incorporate priors and allowances in the analysis. We have included an array of such systematic allowances, with tolerances ranging from optimistic to pessimistic. Our technique differs from the DETF (Albrecht et al. 2006), who use a simpler Fisher matrix approach in the prediction of dark energy constraints. Despite these differences, we have endeavored to make our calculations of the FoM (Section 2) as comparable as possible.

Benchmarking our results against those of the DETF for other, future 'Stage IV' dark energy experiments i.e. large, long-term missions, we find that the f_{gas} experiment should provide a comparable FoM to future ground-based SNIa (FoM=$8-22$), space-based SNIa (FoM=$19-27$), ground-based BAO (FoM=$5-55$), space-based BAO (FoM=$20-42$) and space-based cluster counting (FoM=$6-39$) experiments. Formally, the predicted FoM for the f_{gas} experiment is comparable to 'pessimistic' scenarios for weak lensing experiments discussed by Albrecht et al. (2006), although the value falls short of the most optimistic DETF weak lensing predictions. The tight constraints on Ω_m and Ω_{de} for the f_{gas} experiment will be of importance when used in combination with other techniques. Interestingly, the 'pivot point' for the f_{gas} experiment lies between those of the SNIa and BAO/weak lensing/cluster number count experiments, offering excellent redshift coverage in attempts to pin down the evolution of dark energy.

We conclude that the f_{gas} experiment offers a powerful approach for dark energy work, which should be competitive with and complementary to the best other planned dark energy experiments.

ACKNOWLEDGMENTS

REFERENCES

Albrecht A., et al., 2006, astro-ph/0609591

Allen S. W., Rapetti D. A., Schmidt R. W., Ebeling H., Morris G., Fabian A. C., 2007, astro-ph/0706.0033

Allen S. W., Schmidt R. W., Ebeling H., Fabian A. C., van Speybroeck L., 2004, MNRAS, 353, 457

Allen S. W., Schmidt R. W., Fabian A. C., 2002, MNRAS, 334, L11

Allen S. W., Schmidt R. W., Fabian A. C., Ebeling H., 2003, MNRAS, 342, 287

Astier P., et al., 2005, astro-ph/0510447

Bean R., Dore O., 2004, Phys. Rev., D69, 083503

Benjamin J., et al., 2007, astro-ph/0703570

Bennett C. L., et al., 2003, ApJ S., 148, 1

Bonamente M., Joy M. K., LaRoque S. J., Carlstrom J. E., Reese E. D., Dawson K. S., 2006, ApJ, 647, 25

Bond J. R., Contaldi C. R., Lewis A. M., Pogosyan D., 2004, Int. J. Theor. Phys., 43, 599

Bond J. R., Efstathiou G., 1984, ApJ Lett., 285, L45

Borgani S., Rosati P., Tozzi P., Stanford S. A., Eisenhardt P. R., Lidman C., Holden B., Della Ceca R., Norman C., Squires G., 2001, ApJ, 561, 13

Briel U. G., Henry J. P., Boehringer H., 1992, Astron. Astrophys., 259, L31

Caldwell R. R., Doran M., 2005, Phys. Rev., D72, 043527

Chevallier M., Polarski D., 2001, Int. J. Mod. Phys., D10, 213

Clarkson C., Cortes M., Bassett B. A., 2007, astro-ph/0702670

Cole S., et al., 2005, MNRAS, 362, 505

Cooray A., Hu W., Tegmark M., 2000, ApJ, 540, 1

Copeland E. J., Sami M., Tsujikawa S., 2006, hep-th/0603057

Crain R. A., Eke V. R., Frenk C. S., Jenkins A. J., G. M. I., F. N. J., R. P. F., 2007, Mon. Not. Roy. Astron. Soc., 377, 41

David L. P., Jones C., Forman W., 1995, ApJ, 445, 578

Davis M., Efstathiou G., Frenk C. S., White S. D. M., 1985, ApJ, 292, 371

Davis T. M., et al., 2007, astro-ph/0701510

Doran M., Lilley M., 2002, MNRAS, 330, 965

Ebeling H., Barrett E., Donovan D., Ma C.-J., Edge A. C., van Speybroeck L., 2007, ApJ Lett., 661, L33

Ebeling H., Edge A. C., Henry J. P., 2001, ApJ, 553, 668

Eisenstein D. J., et al., 2005, ApJ, 633, 560

Eke V. R., Navarro J. F., Frenk C. S., 1998, Astrophys. J., 503, 569

Ettori S., Fabian A. C., 1999, MNRAS, 305, 834

Ettori S., Tozzi P., Rosati P., 2003, Astron. Astrophys., 398, 879

Evrard A. E., 1997, MNRAS, 292, 289

Fabian A. C., 1991, MNRAS, 253, 29P

Fabian A. C., et al., 2003, Mon. Not. Roy. Astron. Soc., 344, L43

Fabian A. C., Reynolds C. S., Taylor G. B., Dunn R. J. H., 2005, Mon. Not. Roy. Astron. Soc., 363, 891

Feng B., Wang X.-L., Zhang X.-M., 2005, Phys. Lett., B607, 35

Fosalba P., Gaztanaga E., Castander F., 2003, ApJ, 597, L89

Fukugita M., Hogan C. J., Peebles P. J. E., 1998, Astrophys. J., 503, 518

Gladders M. D., et al., 2007, Astrophys. J., 655, 128

Grego L., Carlstrom J. E., Reese E. D., Holder G. P., Holzapfel W. L., Joy M. K., Mohr J. J., Patel S., 2001, ApJ, 552, 2

Guo Z.-K., Piao Y.-S., Zhang X.-M., Zhang Y.-Z., 2005, Phys. Lett., B608, 177

Henry J. P., 2004, ApJ, 609, 603

Hoekstra H., et al., 2006, Astrophys. J., 647, 116

Hogg D. W., 1999, astro-ph/9905116

Hu W., 2005, Phys. Rev., D71, 047301

Huey G., 2004, astro-ph/0411102

Jarvis M., Jain B., Bernstein G., Dolney D., 2005, astro-ph/0502243

Jenkins A., Frenk C. S., White S. D. M., Colberg J. M., Cole S., Evrard A. E., Couchman H. M. P., Yoshida N., 2001, Mon. Not. Roy. Astron. Soc., 321, 372

Jha S., Riess A. G., Kirshner R. P., 2007, Astrophys. J., 659, 122

Kahya E. O., Onemli V. K., 2006, gr-qc/0612026

Knop R. A., et al., 2003, ApJ, 598, 102

Kodama H., Sasaki M., 1984, Prog. Theor. Phys. Suppl., 78, 1

Kosowsky A., Milosavljevic M., Jimenez R., 2002, Phys. Rev., D66, 063007

Lacey C., Cole S., 1994, MNRAS, 271, 676

LaRoque S. J., Bonamente M., Carlstrom J. E., Joy M. K., Nagai D., Reese E. D., Dawson K. S., 2006, ApJ, 652, 917

Lewis A., 2005, Phys. Rev., D71, 083008

Lewis A., Bridle S., 2002, Phys. Rev., D66, 103511

Lewis A., Challinor A., Lasenby A., 2000, Astrophys. J., 538, 473

Lewis A., Weller J., Battye R., 2006, Mon. Not. Roy. Astron. Soc., 373, 561

Lin Y.-T., Mohr J. J., 2004, Astrophys. J., 617, 879

Lin Y.-T., Mohr J. J., Stanford S. A., 2003, ApJ, 591, 749

Linder E. V., 2003, Physical Review Letters, 90, 091301

Linder E. V., 2006, Astropart. Phys., 26, 102

Ma C.-P., Bertschinger E., 1995, ApJ, 455, 7

Mantz A., Allen S. W., Ebeling H., Rapetti D., 2007, astro-ph/0709.4294

Markevitch M., 1998, ApJ, 504, 27

Million E., et al., 2007, in preparation

Mohr J. J., Mathiesen B., Evrard A. E., 1999, ApJ, 517, 627

Molnar S. M., Birkinshaw M., Mushotzky R. F., 2002, ApJ, 570, 1

Muchovej S., et al., 2007, ApJ, 663, 708

Nagai D., Vikhlinin A., Kravtsov A. V., 2007, Astrophys. J., 655, 98

Onemli V. K., Woodard R. P., 2002, Class. Quant. Grav., 19, 4607

Onemli V. K., Woodard R. P., 2004, Phys. Rev., D70, 107301

Page L., et al., 2003, Astrophys. J. Suppl., 148, 233

Percival W. J., et al., 2007, astro-ph/0705.3323

Perlmutter S., et al., 1999, ApJ, 517, 565

Perotto L., Lesgourgues J., Hannestad S., Tu H., Wong Y. Y. Y., 2006, JCAP, 0610, 013

Planck 2006, astro-ph/0604069

Rapetti D., Allen S. W., Amin M. A., Blandford R. D., 2007, MNRAS, 375, 1510

Rapetti D., Allen S. W., Weller J., 2005, MNRAS, 360, 555

Rassat A., Land K., Lahav O., Abdalla F. B., 2007, Mon. Not. Roy. Astron. Soc., 377, 1085

Reiprich T. H., Böhringer H., 2002, ApJ, 567, 716

Reynolds C. S., McKernan B., Fabian A. C., Stone J. M., Vernaleo J. C., 2005, Mon. Not. Roy. Astron. Soc., 357, 242

Riess A. G., et al., 1998, ApJ, 116, 1009

Riess A. G., et al., 2004, ApJ, 607, 665

Riess A. G., et al., 2007, ApJ, 659, 98

Roussel H., Sadat R., Blanchard A., 2000, Astron. Astrophys., 361, 429

Rozo E., et al., 2007, astro-ph/0703571

Ruhl J., et al., 2004, in Bradford C. M., et al. eds, Millimeter and Submillimeter Detectors for Astronomy II. Vol. 5498 of Society of Photo-Optical Instrumentation Engineers (SPIE) Conference, The South Pole Telescope. pp 11–29

Sanderson A. J. R., Ponman T. J., 2003, MNRAS, 345, 1241

Schmidt R. W., Allen S. W., Fabian A. C., 2004, MNRAS, 352, 1413

Schuecker P., Caldwell R. R., Bohringer H., Collins C. A., Guzzo L., 2003, Astron. Astrophys., 402, 53

Scranton R., et al., 2003, astro-ph/0307335

Sehgal N., Trac H., Huffenberger K., Bode P., 2007, ApJ, 664, 149

Seljak U., et al., 2005, Phys. Rev., D71, 103515

Spergel D. N., et al., 2003, ApJ S., 148, 175

Spergel D. N., et al., 2006, astro-ph/0603449

Tegmark M., Eisenstein D. J., Hu W., de Oliveira-Costa A., 2000, ApJ., 530, 133

Upadhye A., Ishak M., Steinhardt P. J., 2005, Phys. Rev., D72, 063501

Van Waerbeke L., Mellier Y., Hoekstra H., 2005, Astron. Astrophys., 429, 75

Viel M., Weller J., Haehnelt M., 2004, MNRAS, 355, L23

Vikman A., 2005, Phys. Rev., D71, 023515

Voevodkin A., Vikhlinin A., 2004, ApJ, 601, 610

Weller J., Lewis A. M., 2003, MNRAS, 346, 987

White D. A., Fabian A. C., 1995, MNRAS, 273, 72

White S., Navarro J., Evrard A., Frenk C., 1993, Nature, 366, 429

White S. D. M., Frenk C. S., 1991, ApJ, 379, 52

Wood-Vasey W. M., et al., 2007, astro-ph/0701041

Wright E. L., 2007, astro-ph/0701584

Xia J.-Q., Cai Y.-F., Qiu T.-T., Zhao G.-B., Zhang X., 2007, astro-ph/0703202

Xia J.-Q., Zhao G.-B., Feng B., Li H., Zhang X., 2006, Phys. Rev., D73, 063521

Zhao G.-B., Xia J.-Q., Li M., Feng B., Zhang X., 2005, Phys. Rev., D72, 123515